Austin Journal of Pharmacology and Therapeutics

Open Access

Austin Publishing Group

Research Article

Ger-Gen-Chyn-Lian-Tang Alleviated Liver Fibrosis by Reducing M1 Macrophage-Mediated Inflammation Through Downregulation of Osteopontin Expression in Bile Duct Ligation Challenged Mice

Tsai-Jean Lee[1]; Zi-Yu Chang[1,2]; Ru-Yin Tsai[3,4]; Tse-Hung Huang[5-9*]; Chin-Chang Chen[3,4*]

[1]Department of Traditional Chinese Medicine, Chang Gung Memorial Hospital, Keelung, Taiwan

[2]Department of Nursing, Chang Gung University of Science and Technology, Taoyuan, Taiwan.

[3]Department of Anatomy, School of Medicine, Chung Shan Medical University, Taichung, Taiwan

[4]Department of Medical Education, Chung Shan Medical University Hospital, Taichung, Taiwan

[5]Department of Traditional Chinese Medicine, Chang Gung Memorial Hospital, Linkou, Taiwan

[6]School of Chinese Medicine, College of Medicine, Chang Gung University, Taiwan

[7]Research Center for Food and Cosmetic Safety and Research Center for Chinese Herbal Medicine, Chang Gung University of Science and Technology, Taoyuan, Taiwan

[8]Department of Chemical Engineering and Graduate Institute of Biochemical Engineering, Ming Chi University of Technology, New Taipei, Taiwan

[9]Department of Traditional Chinese Medicine, Xiamen Chang Gung Hospital, China

***Corresponding author: Chin-Chang Chen**

Department of Anatomy, School of Medicine, Chung Shan Medical University, Taichung, Taiwan;
Tse-Hung Huang, Department of Traditional Chinese Medicine, Chang Gung Memorial Hospital, Linkou, Taiwan.
Tel: 886-4-36097930; 886-975360763
Email: geoge6211@csmu.edu.tw; huangtehung@gmail.com

Received: July 22, 2024
Accepted: August 15, 2024
Published: August 22, 2024

Abstract

Hepatic macrophages are crucial for defending against infections and are involved in all stages of liver fibrosis. Osteopontin (OPN), a phosphorylated glycoprotein, also contributes to the progression of liver fibrosis. This study aimed to assess whether Ger-Gen-Chyn-Lian-Tang (GGCLT) can reduce liver fibrosis by targeting M1 macrophage-mediated inflammation and lowering OPN levels. Male C57BL/6 mice were assigned to either a sham-control group or a Bile Duct Ligation (BDL) group, with or without GGCLT treatment at doses of 30, 100, and 300 mg/kg. Plasma alanine Aminotransferase (ALT) levels were measured, and liver histopathology and other hepatic parameters were analyzed. In vitro, RAW264.7 macrophages were preincubated with OPN siRNA before being treated with GGCLT and a high Concentration of Chenodeoxycholic Acid (CDCA). BDL mice showed elevated plasma ALT, increased Monocyte Chemoattractant Protein-1 (MCP-1), enhanced macrophage infiltration, and higher levels of M1 macrophage-related inflammatory factors. Additionally, levels of OPN, Nuclear Factor Kappa B (NF-κB), Transforming Growth Factor-β (TGF-β), and α-Smooth Muscle Actin (α-SMA) were significantly elevated. GGCLT treatment at doses of 100 and 300 mg/kg reduced these effects. Furthermore, OPN siRNA preincubation enhanced the ability of 30 μg/ml GGCLT to decrease CDCA-induced increases in TGF-β and M1 macrophage-related inflammatory factors in RAW264.7 cells. In summary, GGCLT alleviated BDL-induced liver fibrosis by reducing M1 macrophage-driven inflammation through downregulation of OPN expression.

Keywords: Ger-Gen-Chyn-Lian-Tang; Bile duct ligation; Macrophage-mediated inflammation; Monocyte chemoattractant protein-1; Osteopontin

Abbreviations: ECM: Extracellular Matrix; HSCs: Hepatic Stellate Cells; TNF-α: Tumor Necrosis Factor-α; IL-6: Interleukin-6; NF-κB: Nuclear Factor-κB; TGF-β: Transforming Growth Factor-β; MCP-1/CCL2: Monocyte Chemoattractant Protein-1/CC Chemokine Ligand 2; CCl_4: Carbon Tetrachloride; OPN: Osteopontin; PSC: Primary Sclerosing Cholangitis; BDL: Bile-Duct Ligation; GGCLT: Ger-Gen-Chyn-Lian-Tang; TAA: Thioacetamide; α-SMA: α-Smooth Muscle Actin; ALT: Alanine Aminotransferase; IF stain: Immunofluorescence Stain; IHC stain: Immunohistochemical Stain; IFN-γ: Interferon-γ; CDCA: Chenodeoxycholic Acid; MMT: Macrophage-to-Myofibroblast Transition

Citation : Lee TJ, Chang ZY, Tsai RY, Huang TH, Chen CC. Ger-Gen-Chyn-Lian-Tang Alleviated Liver Fibrosis by Reducing M1 Macrophage-Mediated Inflammation Through Downregulation of Osteopontin Expression in Bile Duct Ligation Challenged Mice. Austin J Pharmacol Ther. 2024; 12(2): 1191.

Introduction

Hepatic fibrosis manifests through an abundance of extracellular matrix (ECM) deposition, activation of Hepatic Stellate Cells (HSCs), and portal fibroblasts, marking the conclusive route of chronic liver diseases [1]. Fibrotic changes within the liver are initiated by Kupffer cells (resident macrophages) or macrophages derived from monocytes, which can transition phenotypically, perpetuating an inflammatory phase that leads to the extensive release of proinflammatory cytokines [2,3]. Therefore, hepatic macrophages serve as the primary defenders against pathogens and play a crucial role throughout all stages of liver fibrosis, which are involved from the initial inflammation and fibrosis progression to the degradation of fibrillar collagens and the resolution of scars [4]. It is recognized that classically activated macrophages, known as M1 macrophages, play a vital role in triggering both acute and chronic inflammatory responses. Therefore, activated hepatic macrophages and Kupffer cells are major producers of cytokines, releasing Tumor Necrosis factor-α (TNF-α), Interleukin-6 (IL-6), and IL-1β [5-7] *via* signaling pathways dependent on the transcriptional factor Nuclear Factor-κB (NF-κB) [8]. These cytokines serve as significant stimuli for the initiation of fibrogenesis. Additionally, macrophages in the liver produce Transforming Growth Factor-β (TGF-β) and Platelet-Derived Growth Factor (PDGF) during fibrosis development [9]. As a result, macrophages regulate functions of HSCs by secreting profibrogenic cytokines. In response, activated HSCs generate substantial amounts of ECM.

Monocyte Chemoattractant Protein-1/CC Chemokine Ligand 2 (MCP-1/CCL2) acts as a potent attractant for monocytes and plays a role in the pathogenesis of various inflammatory diseases. Furthermore, MCP-1 draws peripheral monocytes to the liver and promotes their transition into the M1 macrophage phenotype within hepatic tissue [10]. After liver injury, proinflammatory monocyte-derived macrophages are attracted to the site of damage due to the presence of MCP-1. This chemokine is produced by fibroblasts, Kupffer cells, activated cholangiocytes, and endothelial cells as part of the body's inflammatory response. Queck et al. suggested that hepatic infiltration of macrophages and MCP-1 level are heightened in mouse liver fibrosis induced by carbon tetrachloride (CCl_4) [11]. Additionally, pharmacological inhibition of MCP-1 diminished liver macrophage infiltration and further improved steatohepatitis in the methionine-choline-deficient diet-fed mice [12].

Osteopontin (OPN) is a phosphorylated glycoprotein secreted by macrophages, monocytes, and activated T lymphocytes, and it plays a significant role in the development of liver fibrosis [13]. Primary Sclerosing Cholangitis (PSC) manifests through the formation of multiple fibroinflammatory strictures in the bile ducts, with macrophages purportedly holding a pivotal position in its progression [14]. A recent report indicated a notable elevation in serum OPN levels among patients in advanced stages of PSC [15]. Remarkably, in mice subjected to Bile-Duct Ligation (BDL), cholestasis-induced fibrosis was marked by the accumulation of monocyte-derived macrophages expressing high levels of OPN in the liver tissues [15]. Additionally, Zheng et al proposed that OPN is crucial for the induction of MCP-1 and Macrophage Inflammatory Protein-1β (MIP-1β) *via* NF-κB and Mitogen-Activated Protein Kinase (MAPK) pathways in the context of rheumatoid arthritis [16].

Ger-Gen-Chyn-Lian-Tang (GGCLT), a formally standardized blend of traditional Chinese herbal remedies, comprises *Puerariae radix*, *Scutellariae radix*, *Coptidis rhizome*, and *Glycyrrhizae radix*. GGCLT treatment was reported to attenuate the advancement of atherosclerosis in apolipoprotein $E^{-/-}$ mice [17]. Our previous studies indicated that GGCLT possessed an anti-liver fibrosis effect by suppressing hepatic oxidative stress, angiogenesis and fibrogenesis, as observed in Thioacetamide (TAA) or BDL-induced mouse model [18, 19]. Additionally, administration of GGCLT mitigates the advancement of nonalcoholic fatty liver disease in *db/db* obese mice by decreasing hepatic lipotoxicity and inflammation [20]. BDL leads to cholestatic injury and periportal biliary fibrosis in the liver by elevating biliary pressure, inducing mild inflammation and generating Reactive Oxygen Species (ROS), ultimately resulting in cholestasis and fibrosis [21]. In addition, perisinusoidal and periportal fibrosis were observed following BDL surgery in rats, characterized by a rapid induction of α-Smooth Muscle Actin (α-SMA) expression and ECM deposition [22, 23]. Enhancing our comprehension of the cellular and molecular pathways involved in the inflammation of liver fibrosis can be achieved using the BDL experimental rodent model. Therefore, this study aims to investigate the potential of GGCLT treatment to alleviate liver fibrosis by reversing hepatic macrophage-mediated inflammation through downregulation of OPN-mediated pathway. This will be achieved using an *in vivo* mouse model challenged with BDL and an *in vitro* macrophage model exposed to the high concentration of bile acid.

Materials and Methods

Preparation of GGCLT

The preparation and formula analysis of GGCLT were conducted in accordance with methods outlined in our previous research [18,19]. In brief, the components of GGCLT, consisting of P. *radix*, S. *radix*, C. *rhizome*, and G. *radix* in a weight ratio of 8:3:3:2, were combined. The initial step involved boiling the mixture at 80°C for 2 h in dH_2O. Following filtration, the resulting mixture was frozen at -80°C, producing a paste crystal residue comprising approximately 12.5 % (w/w). This residue underwent lyophilization at -20°C, yielding a dried compound. Prior to application, the dried compound was reconstituted in dH_2O.

Animals and Experimental Protocols

Male C57BL/6 mice (5-6 weeks old) were purchased from the National Laboratory Animal Center in Taipei, Taiwan and were accommodated in a temperature-regulated setting (20 ± 2°C) with a 12 h light/dark cycle. Experimental procedures for animal studies were conducted as our previous established protocol [19], with minor modifications. The mice were randomly assigned to groups and received either dH_2O or GGCLT at doses of 30, 100, and 300 mg/kg body weight, administered orally once daily for 4 weeks. Initially, the mice were anesthetized with 4 % isoflurane and underwent laparotomy, during which the bile duct was ligated and sectioned. Sham-control mice underwent a similar laparotomy without ligation. Additionally, the sham-control mice were gavage with an equal volume of dH_2O. Plasma and liver samples were collected for analysis after the mice were sacrificed by CO_2 inhalation followed by decapitation. All animal procedures adhered to guidelines from the Chang Gung Memorial Hospital Animal Care and Use Committee (IACUC No. 2016060603).

Cell Culture and *in vitro* Chenodeoxycholic Acid Treatment

RAW264.7 mouse macrophage-derived cell line was obtained from the Food Industry Research and Development Institute (Hsinchu, Taiwan). Cultured in Dulbecco's Modified Eagle's

Medium (DMEM) supplemented with 10 % Fetal Bovine Serum (FBS) and 1 % penicillin/streptomycin, cells were maintained at 37°C in a 5 % CO_2 humidified incubator. For Chenodeoxycholic Acid (CDCA) administration, cells were seeded in 6-well plates at a density of 10^6 cells/well and treated with 100 µM CDCA for a duration of 24 h.

Cytokine Assay

Plasma Alanine Aminotransferase (ALT) levels were assessed with a diagnostic kit from Randox Laboratories, Antrim, UK, as per the manufacturer's instructions.

Histological and Cell Immunofluorescence Stains

Liver histological assessments were conducted with Hematoxylin and Eosin (H&E), Masson's trichrome and Immunohistochemical (IHC) stains, according to our previous protocols [24]. Briefly, liver tissues were fixed in 4 % paraformaldehyde, paraffin-embedded, and sectioned into 5-µm-thick slices. Staining was done using H&E and Masson's trichrome stain kit (Sigma-Aldrich) in accordance with the manufacturer's instructions. For IHC stain, tissue sections were deparaffinized and treated with 0.3 % H_2O_2 to block endogenous peroxidase activity. Primary antibodies (anti-F4/80, anti-MCP-1, anti-OPN, anti-NF-κB and anti-α-SMA from Santa Cruz Biotechnology) were incubated at 4°C overnight. Biotinylated secondary antibodies and avidin-biotin complex reagent were subsequently added, followed by color development with 3,3'-Diaminobenzidine (DAB). For NF-κB Immunofluorescence (IF) stain, RAW264.7 cells were seeded onto glass coverslips, incubated with anti-NF-κB at 4°C overnight, and then with goat anti-rabbit FITC secondary antibody. DAPI was used for nuclear staining. After fixation in 4 % paraformaldehyde for 15 mins, the images were visualized using a fluorescence microscope.

Real-Time Quantitative PCR (RT-qPCR) Assay

Total RNA was isolated with the EasyPrep Total RNA Kit (BioTools Co., LTD, Taiwan). Complementary DNA (cDNA) was synthesized from 5 µg of total RNA using the RevertAid First Strand cDNA Synthesis kit (Thermo Fisher Scientific). Real-time PCR was conducted with the SYBR system on a LightCycler 1.5 (Roche Applied Science, Mannheim, Germany). The CT values of each gene were normalized to CT values of GAPDH. Primer sequences are listed in Table 1.

Western Blot Measurement

Liver tissues or RAW264.7 cells were lysed in 0.2 ml of Cel-Lytic MT Lysis Reagent (Sigma-Aldrich) supplemented with 1% phosphatase inhibitor cocktail and protease inhibitor cocktail, followed by centrifugation at 13,000 x g for 30 min at 4°C. Additionally, nuclear fraction isolation was performed using a nuclear isolation kit (Abcam, Cambridge, MA, USA) as per the manufacturer's instructions. Protein concentration in the lysate was determined using the Bradford assay. Subsequently, the lysates underwent sodium dodecyl sulfate-polyacrylamide gel electrophoresis (SDS-PAGE) and were transferred to Polyvinylidene Fluoride (PVDF) membranes. After incubation with primary antibodies against MCP-1, OPN, NF-κB, H1 and β-actin (all purchased from Santa Cruz Biotechnology), horseradish peroxidase-conjugated secondary antibodies were applied, and the resulting reaction was visualized using an electrochemiluminescence kit. Data normalization was performed with H1 and β-actin as internal controls.

Small Interfering RNA (siRNA) Against OPN

The OPN gene was silenced with Dharmacon™ siRNA (GE Dharmacon, Lafayette, CO, USA) according to the manufacturer's instructions. The siRNA duplex nucleotides were designed based on the method of Wang [25] for the specific silencing of OPN: siRNA1, 5'-TAGACCCCATGGAGTGGCA-3'; siRNA2, 5'-GGTGGCACAGCCACTGACA-3'; siRNA3, 5'-ACCGTCTGGAGGCTGTTCA-3'; and a scrambled control, 5'-CATGGAGTGGCACGTAGGT-3'. The Raw264.7 cells were transfected using DharmaFECT 1 transfection reagent combined with either 100 nM OPN or scrambled control siRNA duplex in the DMEM culture medium without antibiotics for 72 h.

Statistical Analysis

Mean ± S.E.M. values were analyzed using Student's *t*-tests for pairwise group comparisons. For the results of the RAW264.7 cell *in vitro* experiment, data are presented as mean ± S.E.M. of at least 3 independent experiments. For multiple group comparisons, one-way Analysis of Variance (ANOVA) was used, followed by Tukey's post hoc tests for further analysis. Different symbols or letters indicated statistically significant differences ($P < 0.05$).

Results

GGCLT Treatment Alleviated Liver Injury in the BDL-Challenged Mice

As illustrated in the upper panel of Figure 1, the liver tissues of BDL mice, in contrast to those of the sham-control mice, exhibited an enlarged appearance and dark brown patches, lacking the bright blood coloration typically associated with healthy liver tissue. Meanwhile, H&E stain revealed significant hepatoatrophy and extensive coagulation necrosis in the liver tissues of mice following BDL administration (Figure 1A, middle panel). Moreover, a clear increase in plasma ALT level was observed in the BDL mice compared to the sham-control groups (Figure 1B). In addition, Masson-trichrome stain revealed a distinct pattern of collagen fiber deposition around the central veins and portal areas, accompanied by the development of portal-portal septa in the mice after BDL challenge (Figure 1A, lower panel). Furthermore, administration of GGCLT at doses of 300 mg/kg notably mitigated these effects in mice afflicted with BDL-induced liver fibrosis (Figure 1).

Table 1: Primer sequences used for quantitative RT-qPCR analysis.

Gene	Forward	Reverse
TNF-α	TTGACCTCAGCGCTGAGTTG	CCTGTAGCCCACGTCGTAGC
IFN-γ	AGGCTCACGTCACCAAGTCCC	TGGTCTCGAAAGCTACGTGGGAGG
IL-6	TGGAGTCACAGAAGGAGTGGCTAAG	TCTGACCACAGTGAGGAATGTCCAC
IL-1β		TCTTCTTTGGGTATTGCTTGG
TGF-β	TGTAATGAAAGACGGCACACCTGCCCTCTACAACCAACACAACCCG	AACTGCTCCACCTTGGGCTTGCGAC
α-SMA	CCACCGCAAATGCTTCTAAGTGGTCCCAAAGGTGCTGATGG	GGCAGGAATGATTTGGAAAGGGACCAGCCTCACCACGGTCT
Procollagen-I		
Procollagen-III	CCCCTGGTCCCTGCTGTGG	GAGGCCCGGCTGGAAAGAA
GAPDH	TCACCACCATGGAGAAGGC	GCTAAGCAGTTGGTGGTGCA

TNF-α, tumor necrosis factor-α; IFN-γ, interferon-γ; IL-6, interleukin-6; IL-1β, interleukin-1β; TGF-β, transforming growth factor-β; α-SMA, α-smooth muscle actin; GAPDH, glyceraldehyde 3-phosphate dehydrogenase.

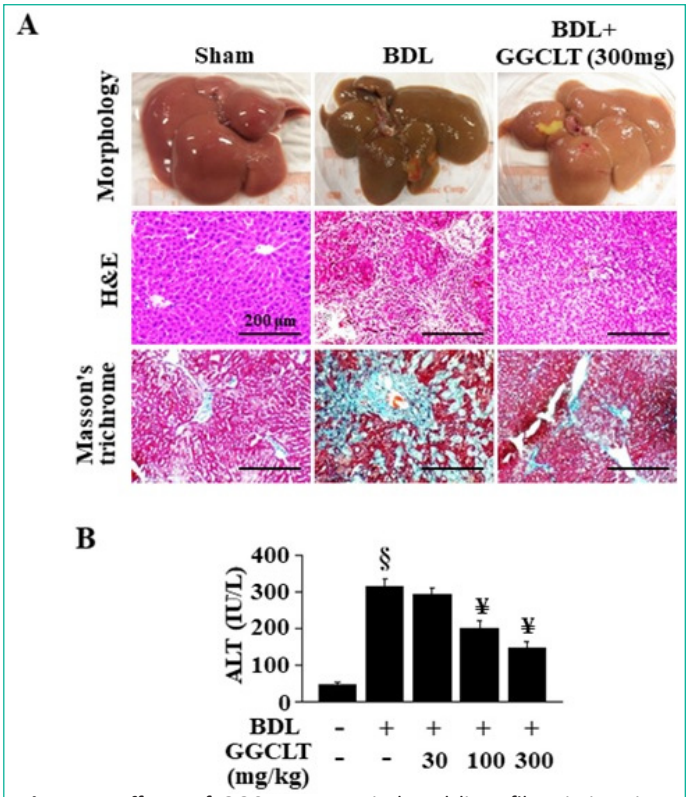

Figure 1: Effects of GGCLT on BDL-induced liver fibrosis in mice. (A) upper plane: the liver morphology after mice sacrifice; middle plane: paraffin-embedded liver sections underwent staining procedures by using H&E; lower plane: Masson's trichrome stain. All results of H&E and Masson's trichrome stains were shown at 200 x magnification and the length of scale bar was indicated as 200 μm. (B) Plasma ALT levels were measured after mice sacrifice in the BDL + GGCLT groups. The data are expressed as the mean ± S.E.M. § P < 0.05 vs. sham-control mice (n=7); $^{¥}$ P < 0.05 vs. BDL mice (n=7).

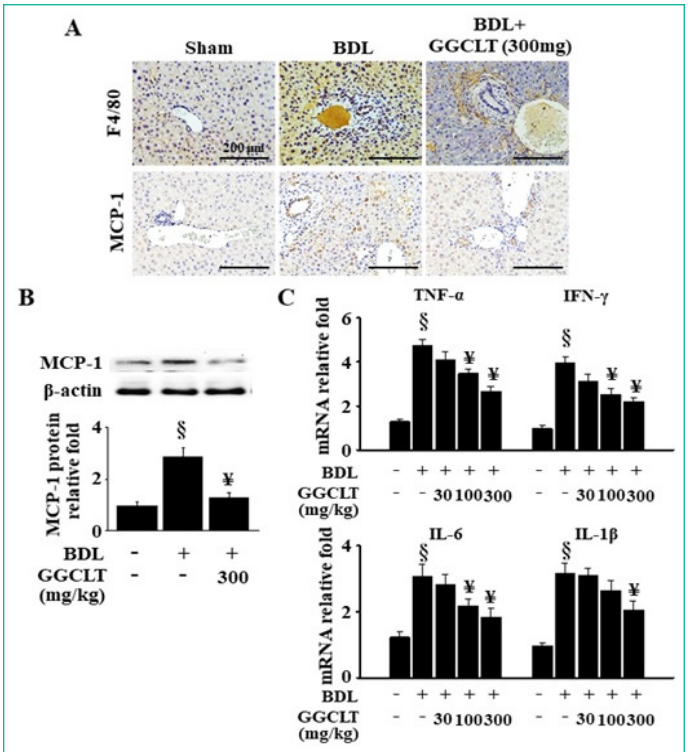

Figure 2: GGCLT reduced the infiltration of macrophages and the inflammatory responses in the liver tissues of mice caused by BDL. (A) Liver tissues from sham-control and BDL mice treated without or with 300 mg/kg GGCLT were stained with antibodies of F4/80 (upper plane) and MCP-1 (lower plane), respectively. The results were shown at 200 x magnification and the length of scale bar was indicated as 200 μm. (B) The protein level of the MCP-1 in the liver tissues were detected by Western blot. (C) The mRNA levels of TNF-α, IFN-γ, IL-6 and IL-1β were determined by RT-qPCR. The data are expressed as the mean ± S.E.M. § P < 0.05 vs. sham-control mice (n=7); $^{¥}$ P < 0.05 vs. BDL mice (n=7).

Effect of GGCLT on Macrophage-Mediated Inflammation in the Liver of BDL Mice

As shown in Figure 2A, there was a notable increase in the recruitment of macrophages, indicated by F4/80 stain, to the liver following BDL treatment in mice. Additionally, there was a significant upregulation of MCP-1 expression observed in the BDL-challenged mice. The protein level of MCP-1 was significantly elevated in the liver tissues of BDL-challenged mice as well (Figure 2B). Conversely, the treatment of 300 mg/kg GGCLT decreased the BDL-induced hepatic enhancement of macrophages infiltration and MCP-1 expression in mice (Figure 2A & 2B). Furthermore, following BDL induction (Figure 2C), there was a notable increase observed in the hepatic mRNA levels of TNF-α, interferon-γ (IFN-γ), IL-6 and IL-1β, all indicative of inflammation. However, these increases were significantly suppressed by GGCLT treatment at dosages of 100 and 300 mg/kg (Figure 2C).

Effect of GGCLT on Hepatic OPN Level in the BDL-Challenged Mice

As shown in Figure 3A, BDL-administrated mice showed an obvious upregulation in the OPN level of the liver tissue in comparison of sham-control mice. In addition, the results of Western blot showed that hepatic protein level of OPN was significantly elevated in the BDL-challenged mice as well (Figure 2B), and these effects were suppressed by treatment with 300 mg/kg GGCLT.

Effect of GGCLT on BDL-Induced Hepatic NF-κB Level in Mice

The results of IHC stain and Western blot showed that hepatic level of NF-κB was obviously increased after BDL administration compared with show-control mice. Remarkably, treatment with 300 mg/kg GGCLT effectively suppressed these effects (Figure 4).

GGCLT treatment Reduced the Fibrogenesis-Related Factors in the Liver of BDL Mice

The result of IHC stain showed that the α-SMA level in the liver tissues was obvious increased in the BDL mice (Figure 5A). A further enhancement was observed in hepatic mRNA levels of TGF-β, α-SMA, procollagen-I and procollagen-III in the mice after BDL administration compared to the sham-control mice (Figure 5B). In contrast, treatment with GGCLT at 100 and 300 mg/kg significantly inhibited BDL-induced these effects (Figure 5).

Synergistic Effect of OPN Gene Silencing on GGCLT Reduced CDCA-Induced the Elevated mRNA Levels of TGF-β and Inflammation-Related Factors in the RAW264.7 Cells

A recent study demonstrated a notable increase in serum Chenodeoxycholic Acid (CDCA) levels, a primary bile acid produced in the liver tissues of BDL mice [26]. To replicate the elevated levels of MCP-1 and OPN observed in our BDL mice, RAW264.7 macrophages were cultured in a medium with a high concentration of CDCA. This approach aimed to investigate whether GGCLT could reduce the BDL-induced rise in hepatic levels of TGF-β and inflammation, potentially by inhibiting OPN expression. The results of IF stain showed that NF-κB level was enhanced after exposure to 100 μM CDCA compared to a CDCA-free medium, and this effect was reversed by treatment with 30 μg/ml GGCLT (Figure 6A). Additionally, 30 μg/ml GGCLT sig-

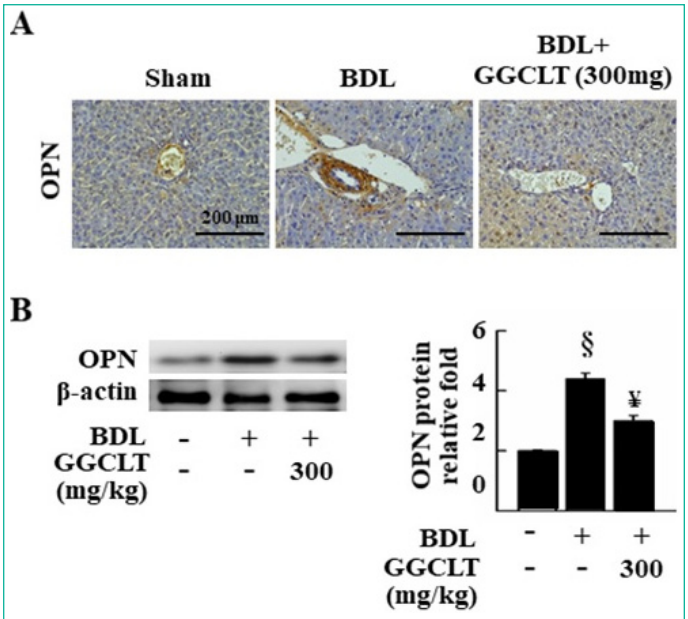

Figure 3: GGCLT lowered the levels of OPN in the liver tissues of mice induced by BDL. (A) Liver sections from sham-control, and BDL-challenged mice treated without or with 300 mg/kg GGCLT, were stained with the OPN antibody. The results were shown at 200 x magnification and the length of scale bar was indicated as 200 μm. (B) The protein level of OPN in the liver tissues were detected by Western blot. The data are expressed as the mean ± S.E.M. § P < 0.05 vs. sham-control mice (n=7); $^{¥}$ P < 0.05 vs. BDL group (n=7).

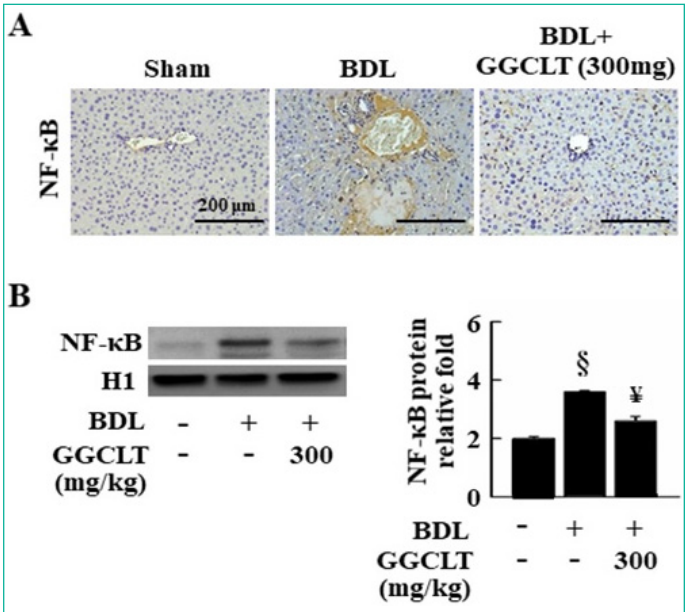

Figure 4: GGCLT decreased hepatic level of NF-κB in the BDL-challenged mice. (A) Liver sections from sham-control and BDL-challenged mice treated without or with 300 mg/kg GGCLT were stained with the NF-κB antibody. The results were shown at 200 x magnification and the length of scale bar was indicated as 200 μm. (B) The nuclear protein level of NF-κB in the liver tissues were detected by Western blot. The data are expressed as the mean ± S.E.M. § P < 0.05 vs. sham-control mice (n=7); $^{¥}$ P < 0.05 vs. BDL mice (n=7).

nificantly suppressed the CDCA-induced increase in MCP-1 and OPN protein levels in RAW264.7 cells (Figure 6B).

Subsequently, The OPN protein level was reduced by approximately 70% in RAW264.7 cells incubated with 100 nM OPN siRNA for 72 h compared to the scrambled control group (Figure 6C). Moreover, preincubation with OPN siRNA synergistically enhanced the ability of 30 μg/ml GGCLT to inhibit the CDCA-induced increase in the mRNA levels of TGF-β, TNF-α, IFN-γ, IL-6, and IL-1β (Figure 6D).

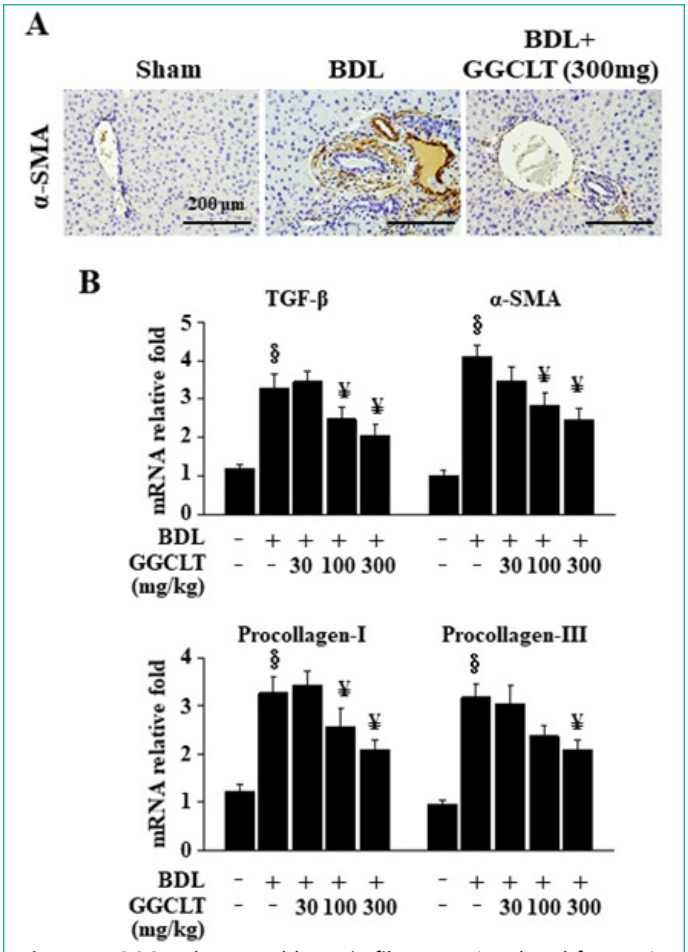

Figure 5: GGCLT decreased hepatic fibrogenesis-related factors in the BDL–challenged mice. (A) Representative IHC stain for α-SMA in the sham-control and BDL-challenged mice treated without or with 300 mg/kg GGCLT. The results were shown at 200 x magnification and the length of scale bar was indicated as 200 μm. (B) The mRNA levels of the TGF-β, α-SMA, Procollagen-I and Procollagen-III in the liver tissues of sham-control and BDL mice in the presence and absence of GGCLT treatment were detected by RT-qPCR. The data are expressed as the mean ± S.E.M. § P < 0.05 vs. sham-control mice for BDL group (n=7); $^{¥}$ P < 0.05 vs. BDL mice (n=7).

Discussion

Based on Traditional Chinese Medicine (TCM) treatment principles, GGCLT is designed to "clear heat and detoxify." Clinical applications of GGCLT encompass treating acute bacterial infections, acute gastroenteritis, and alleviating hangover symptoms. Contemporary studies have unveiled the multifaceted effects of GGCLT including antipyretic, antibacterial, antioxidant, anti-inflammatory properties, and its potential to ameliorate metabolic syndrome. Our previous studies have demonstrated anti-liver fibrotic properties of GGCLT by inhibiting intrahepatic oxidative stress and angiogenesis in mice models subjected to TAA and BDL challenges [18,19]. Upon eliminating the causative factor of liver fibrosis, a correlated reduction appeared in the generation of pro-inflammatory cytokines, heightening collagenolytic activity, and the inhibition of ECM synthesis [27]. The critical role in the pathogenesis of liver fibrosis is attributed to the activation of TGF-β-producing macrophages and the subsequent upregulation of inflammation. MCP-1, secreted by both Kupffer cells and HSCs, aids in the recruitment of immature monocyte-derived macrophages to the liver [12]. Furthermore, OPN is highlighted as a chemoattractant for macrophages in inflammatory liver diseases [28]. Our findings demonstrated that GGCLT treatment mitigated liver fibrosis triggered by BDL challenges by attenuating the macrophage-driven upregulation of

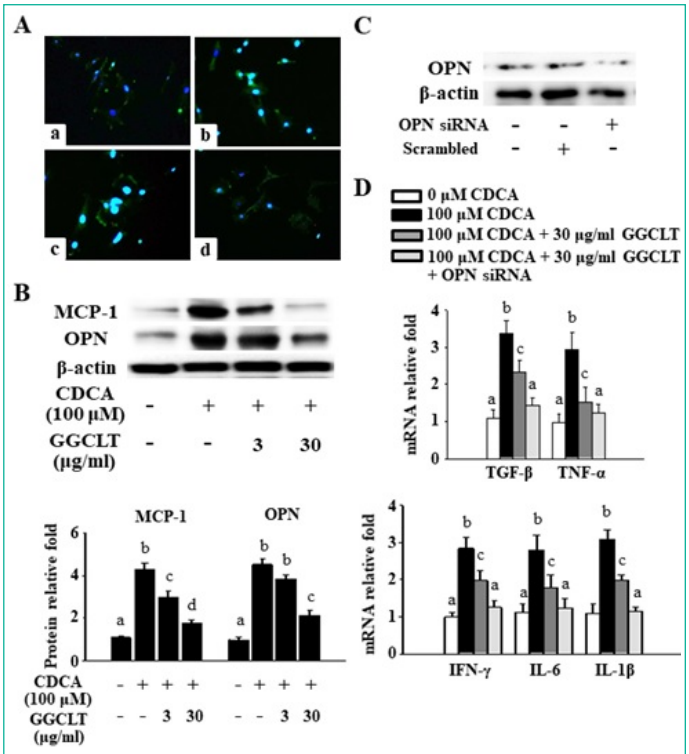

Figure 6: The genetic ablation of OPN synergistically enhanced GGCLT's reduction of the TGF-β mRNA level and inflammatory responses caused by CDCA challenge in RAW264.7 cells. GGCLT was pre-treated at dosages of 3 and 30 μg/ml for 2 h before being co-incubated with 100 μM CDCA for 24 h. (A) The NF-κB level was stained and visualized by fluorescence microscopy. (a) CDCA-free; (b) 100 μM CDCA; (c) 100 μM CDCA + 3 μg/ml GGCLT; (d) 100 μM CDCA + 30 μg/ml GGCLT. The results were shown at 200 x magnification. (B) The protein levels of MCP-1 and OPN were detected by Western blot. (C) Altered expression of OPN protein after the OPN siRNA was introduced into RAW264.7 cells via transient transfection. (D) The mRNA levels of TGF-β, TNF-α, IFN-γ, IL-6 and IL-1β analyzed by RT-qPCR after OPN gene ablation followed by exposure to 30 μg/ml GGCLT plus 100 μM CDCA for 24 h. The results are represented as the mean ± S.E.M. for at least 3 experiments, with different letters indicating statistically significant differences.x magnification and the length of scale bar was indicated as 200 μm. (B) The nuclear protein level of NF-κB in the liver tissues were detected by Western blot. The data are expressed as the mean ± S.E.M. § P < 0.05 vs. sham-control mice (n=7); $^{¥}$ P < 0.05 vs. BDL mice (n=7).

inflammatory responses and enhancing the expression levels of OPN. Additionally, the transcriptional activation of NF-κB is implicated in these mechanisms underlying BDL-induced liver fibrosis in mice. There has been limited research into the relationship between macrophage infiltration and increased OPN expression during the development of hepatotoxic liver injury and cholestatic liver fibrosis. As far as we know, this study is the first to demonstrate that GGCLT reduces BDL-induced liver fibrosis in mice by decreasing macrophage-mediated inflammation and OPN level.

Macrophages found across various tissues undergo polarization in response to environmental cues, giving rise to distinct macrophage subtypes such as M1 and M2 macrophages [29]. Fibrotic changes in the liver are largely driven by Kupffer cells and/or recruited macrophages [2]. The classical activation of M1 macrophages involves the secretion of proinflammatory cytokines such as TNF-α, IL-6, IL-1, and IL-12 [30], playing a crucial role in triggering fibrogenesis. Our findings regarding histopathological features and mRNA expression of proinflammatory cytokines indicate a significant accumulation of macrophages (marked by F4/80) in the terminal hepatic venule and/or portal vein of liver tissues, as observed in mice subjected to BDL compared to sham-control mice. Moreover, hepatic mRNA levels of TNF-α, IFN-γ, IL-6, and IL-1β were notably elevated in these mice. Plasma ALT level was also markedly raised in the BDL-challenged mice compared with sham-control mice. It could be speculated that the macrophage polarization observed in the liver tissues following BDL challenges aligns with the M1 phenotype based on our current study. The similar result was observed in the studies of Xie et al. [31]. Moreover, the influx of inflammatory and fibrogenic monocytes is contingent upon the interaction between MCP-1/CCL2 and its receptor, CCR2 [32]. Inhibiting MCP-1 pharmacologically leads to a reduction in liver fibrosis in murine models [12]. In the context of liver fibrosis, activated HSCs emerge as the primary origin of myofibroblasts, initiating ECM deposition and fostering liver desmoplasia *via* the secretion of collagen-I and α-SMA [33]. Nevertheless, contemporary investigations propose an involvement of macrophages in the process of macrophage-to-myofibroblast transition (MMT), particularly evident in mice experiencing CCl_4-induced liver fibrosis [34]. Our results suggest that the increase in hepatic MCP-1 protein levels observed in mice treated with BDL may be initiated by M1 macrophages. This activation could potentially promote substantial monocyte infiltration into fibrotic livers by inducing the trans differentiation of MMT. Such a process offers a swift and temporary mechanism to amplify the macrophage population in the liver through inflammation-sensitive phagocytes, and these phenomena could be reversed by GGCLT treatment.

A study conducted by Kawashima and colleagues demonstrated that OPN plays a role in facilitating the infiltration of macrophages into necrotic regions in rats following CCl_4 poisoning [35]. Additionally, in a mouse model challenged with BDL, Obeticholic Acid (OCA), a 6-ethyl derivative of CDCA, was found to boost OPN and Thr-OPN expression in the liver, particularly in the portal area [36]. In line with the findings of Wang et al. [36], the histological presence of OPN in the portal area of liver tissues showed a significant increase in our mouse model challenged with BDL compared to sham-control mice. Conversely, our IHC stain results revealed a notable elevation in the OPN level within the portal triad of liver tissues in mice challenged to BDL compared to sham-control mice. The reversal of BDL-induced liver fibrosis by GGCLT could be accompanied by a notable decrease in OPN levels, which may consequently hinder the infiltration of macrophages into necrotic liver regions; however, more evidence is needed to support this speculation.

It was reported that YC-1, identified as a HIF-1α inhibitor, mitigates liver fibrosis induced by BDL in a murine model was attributed to the reduction in HIF-1α-mediated recruitment of inflammatory cells such as neutrophils and macrophages, suppression of angiogenesis, and downregulation of fibrogenesis markers including TGF-β R1, α-SMA, procollagen-I, and procollagen-III [37]. Notably, NF-κB transcriptional activations were implicated in these processes [37]. In this study, an obvious reduction was observed in the macrophage infiltration and hepatic levels of TGF-β, α-SMA, procollagen-I and procollagen-III following administration of 300 mg/kg of GGCLT in mice subjected to BDL. For our mice challenged with BDL, we speculated that inflammation driven by M1 macrophages could have stimulated HSCs to produce collagen, leading to liver fibrosis. GGCLT appeared to reduce these effects. Hence, future investigations should elucidate the mechanisms underlying the MMT process, potentially expanding the application of GGCLT treatment to ameliorate liver fibrosis.

Bile acids have a significant influence on modulating macrophage reactions, suggesting a shift in macrophage functionality within the context of cholestatic liver disease [38]. Chenodeoxycholic Acid (CDCA), a hydrophobic bile acid subtype implicated in cholestatic liver damage, triggers NLRP3 inflammasome activation and subsequent IL-1β secretion in murine macrophages [39]. This process could represent a crucial mechanism driving inflammatory macrophage activation in cholestatic liver disorders, particularly in monocyte-derived macrophages. Our study demonstrated that the high concentration of CDCA led to the upregulation of NF-κB, MCP-1 and OPN expression utilizing the RAW264.7 macrophage *in vitro* model. Meanwhile, treatment with 30 μg/ml GGCLT attenuated these observed effects. Notably, increased levels of MCP-1 in the liver tissues signified macrophage activation. Thus, we speculate that GGCLT treatment may reduce the activation of macrophages induced by toxic bile Acids (CDCA), which is closely associated with MCP-1 expression in our RAW264.7 cell model. Importantly, by silencing the OPN gene using siRNA, we provided in vitro evidence showing that GGCLT treatment reduced the high concentration of CDCA-induced upregulation of TGF-β level and inflammation-related factors, potentially through the inhibition of OPN in RAW264.7 macrophages. However, a limitation of our study is that we did not conduct a converse validation of GGCLT's effect on neutralizing CDCA-aggravated, macrophage-mediated inflammation in RAW264.7 macrophages through the OPN-related pathway using conditional knockin of OPN mRNA.

Puerarin, baicalin, berberine, and glycyrrhiza have been stated as active components found in *Puerariae radix*, *Scutellariae radix*, *Coptisis rhizome*, and *Glycyrrhiza radix*, respectively [40-43]. Previous reports have suggested that puerarin and baicalin possess the ability to mitigate obesity and its associated issues, such as insulin resistance, in mice. This function is achieved by inhibiting inflammatory M1 Adipose Tissue Macrophages (ATM) and enhancing anti-inflammatory M2 ATM level, respectively [44,45]. Furthermore, Berberine has been shown to inhibit inflammation induced by free fatty acids and LPS through modulating the Endoplasmic Reticulum (ER) stress response in both macrophages and hepatocytes [46].

Conclusion

Our findings suggest that GGCLT treatment effectively reduces liver fibrosis by reversing hepatic macrophage-mediated inflammation. This is accomplished by suppressing hepatic levels of MCP-1 and OPN, involving the NF-κB-related mechanism, as demonstrated in the BDL-induced liver fibrosis mouse model.

Author Statements

Author Contributions

T.-J.L., T.-H.H., and C.-C.C. conducted the experiments and authored most of the manuscript. Z.-Y.C. carried out additional experiments and contributed to a minor section of the manuscript. R.-Y. T was responsible for data analysis and preparing the figures. T.-H.H. and C.-C.C. originated the initial concept. All authors reviewed and approved the final manuscript. Additionally, all authors have reviewed and agreed to the journal's authorship agreement.

Funding Sources

This work was supported by Chang Gung Memorial Hospital Research Foundation, Taiwan (grant nos. CMRPG2M0101 and CMRPG3N0571A) and Chung Shan Medical University, Taichung, Taiwan (grant nos. RD11211). The funding source had no role in the study design; in the collection, analysis and interpretation of data; in the writing of the report; or in the decision to submit the article for publication.

Conflict of Interest

The authors declare that they have no conflict of interest to declare.

Availability of Data and Materials

The datasets used and/or analyzed during the current study are available from the corresponding author on reasonable request.

References

1. Friedman SL. Liver fibrosis -- from bench to bedside. J Hepatol. 2003; 38: S38-53.
2. Dou L, Shi X, He X, Gao Y. Macrophage Phenotype and Function in Liver Disorder. Front Immunol. 2020; 10: 3112.
3. Matsuda M, Seki E. Hepatic Stellate Cell-Macrophage Crosstalk in Liver Fibrosis and Carcinogenesis. Semin Liver Dis. 2020; 40: 307-320.
4. Campana L, Iredale JP. Regression of liver fibrosis. in Seminars in liver disease. Semin Liver Dis. 2017; 37: 1-10.
5. Luedde T, Liedtke C, Manns MP, Trautwein C. Losing balance: cytokine signaling and cell death in the context of hepatocyte injury and hepatic failure. Eur Cytokine Netw. 2002; 13: 377-83.
6. Streetz K, Leifeld L, Grundmann D, Ramakers J, Eckert K, Spengler U, et al. Tumor necrosis factor alpha in the pathogenesis of human and murine fulminant hepatic failure. Gastroenterology. 2000; 119: 446-60.
7. Streetz KL, Tacke F, Leifeld L, Wüstefeld T, Graw A, Klein C, et al. Interleukin 6/gp130-dependent pathways are protective during chronic liver diseases. Hepatology. 2003; 38: 218-29.
8. Pradere JP, Kluwe J, Minicis SD, Jiao JJ, Gwak GY, Dapito DH, et al. Hepatic macrophages but not dendritic cells contribute to liver fibrosis by promoting the survival of activated hepatic stellate cells in mice. Hepatology. 2013; 58: 1461-1473.
9. Wynn TA. Cellular and molecular mechanisms of fibrosis. J Pathol. 2008; 214: 199-210.
10. Li L, Wei W, Li Z, Chen H, Li Y, Jiang W, et al. The spleen promotes the secretion of CCL2 and supports an M1 dominant phenotype in hepatic macrophages during liver fibrosis. Cell Physiol Biochem. 2018; 51: 557-574.
11. Queck A, Bode H, Uschner FE, Brol MJ, Graf C, Schulz M, et al. Systemic MCP-1 Levels Derive Mainly from Injured Liver and Are Associated With Complications in Cirrhosis. Front Immunol. 2020; 11: 354.
12. Baeck C, Wehr A, Karlmark KR, Heymann F, Vucur M, Gassler N, et al. Pharmacological inhibition of the chemokine CCL2 (MCP-1) diminishes liver macrophage infiltration and steatohepatitis in chronic hepatic injury. Gut. 2012; 61: 416-26.
13. Song Z, Chen W, Athavale D, Ge X, Desert R, Das S, et al. Osteopontin Takes Center Stage in Chronic Liver Disease. Hepatology. 2021; 73: 1594-1608.
14. Guicciardi ME, Trussoni CE, Krishnan A, Bronk SF, Lorenzo Pisarello MJ, O'Hara SP, et al. Macrophages contribute to the pathogenesis of sclerosing cholangitis in mice. J Hepatol. 2018; 69: 676-686.

15. De Muynck K, Heyerick L, De Ponti FF, Vanderborght B, Meese T, Campenhout SV, et al. Osteopontin characterizes bile duct-associated macrophages and correlates with liver fibrosis severity in primary sclerosing cholangitis. Hepatology. 2024; 79: 269-288.

16. Zheng W, Li R, Pan H, He D, Xu R, Guo T, et al. Role of osteopontin in induction of monocyte chemoattractant protein 1 and macrophage inflammatory protein 1β through the NF-κB and MAPK pathways in rheumatoid arthritis. Arthritis Rheum. 2009; 60: 1957-1965.

17. Ho F, Liao Y, Yang A, Lee Chao PD, Hou Y, Huang C, et al. Anti-atherosclerotic action of Ger-Gen-Chyn-Lian-Tang and AMPK-dependent lipid lowering effect in hepatocytes. J Ethnopharmacol. 2012; 142: 175-87.

18. Chang ZY, Lee TY, Huang TH, Wen CK, Chien RN, Chang HH. Hepatoprotective effects of Ger-Gen-Chyn-Lian-Tang in thioacetamide-induced fibrosis in mice. J Chin Med Assoc. 2014; 77: 360-6.

19. Chang ZY, Chen CC, Liu HM, Yeh YC, Lin TY, Lee TY, et al. Positive Effects of Ger-Gen-Chyn-Lian-Tang on Cholestatic Liver Fibrosis in Bile Duct Ligation-Challenged Mice. Int J Mol Sci. 2019; 20: 4181.

20. Wang CH, Liu HM, Chang ZY, Lee MC, Hsu CH, Lee TY, et al. Antioxidants Rich Herbal Formula Ger-Gen-Chyn-Lian-Tang Protects Lipotoxicity and Ameliorates Inflammation Signaling through Regulation of Mitochondrial Biogenesis and Mitophagy in Non-alcoholic Fatty Liver Disease Mice. Front Biosci (Landmark Ed). 2022; 27: 242.

21. Weiskirchen R, Weiskirchen S, Tag CG Meurer SK. Induction of Obstructive Cholestasis in Mice. Methods Mol Biol. 2023; 2669: 163-175.

22. Tuchweber B, Desmoulière A, Bochaton-Piallat ML, Rubbia-Brandt L, Gabbiani G. Proliferation and phenotypic modulation of portal fibroblasts in the early stages of cholestatic fibrosis in the rat. Lab Invest. 1996; 74: 265-278.

23. Desmoulière A, Darby I, Costa AM, Raccurt M, Tuchweber B, Sommer P, et al. Extracellular matrix deposition, lysyl oxidase expression, and myofibroblastic differentiation during the initial stages of cholestatic fibrosis in the rat. Lab Invest. 1997; 76: 765-778.

24. Chen CC, Chang ZY, Tsai FJ, Chen SY. Resveratrol Pretreatment Ameliorates Concanavalin A-Induced Advanced Renal Glomerulosclerosis in Aged Mice through Upregulation of Sirtuin 1-Mediated Klotho Expression. Int J Mol Sci. 2020; 21: 6766

25. Wang Z, Cui Y, Li W, Chen S, Liu T. Lentiviral-mediated siRNA targeted against osteopontin suppresses the growth and metastasis of gastric cancer cells. Oncol Rep. 2011; 25: 997-1003.

26. Qin T, Hasnat M, Wang Z, Hassan H, Zhou Y, Yuan Z. Geniposide alleviated bile acid-associated NLRP3 inflammasome activation by regulating SIRT1/FXR signaling in bile duct ligation-induced liver fibrosis. Phytomedicine. 2023; 118: 154971.

27. Bataller R, Brenner DA. Liver fibrosis. J Clin Invest. 2005; 115: 209-18.

28. Wen Y, Jeong S, Xia Q, Kong X. Role of Osteopontin in Liver Diseases. Int J Biol Sci. 2016; 12: 1121-8.

29. Martinez FO, Gordon S. The M1 and M2 paradigm of macrophage activation: time for reassessment. F1000Prime Rep. 2014; 6: 13.

30. Trinchieri, G. Interleukin-12 and the regulation of innate resistance and adaptive mmunity. Nat Rev Immunol. 2003; 3: 133-46.

31. Xie C, Wan L, Li C, Feng Y, Kang YJ. Selective suppression of M1 macrophages is involved in zinc inhibition of liver fibrosis in mice. J Nutr Biochem. 2021; 97: 108802.

32. Miura K, Yang L, Rooijen NV, Ohnishi H, Seki E. Hepatic recruitment of macrophages promotes nonalcoholic steatohepatitis through CCR2. Am J Physiol Gastrointest Liver Physiol. 2012; 302: G1310-21.

33. Karin D, Koyama Y, Brenner D, Kisseleva T. The characteristics of activated portal fibroblasts/myofibroblasts in liver fibrosis. Differentiation. 2016; 92: 84-92.

34. Xia S, Huang Y, Zhang Y, Zhang M, Zhao K, Han P. Role of macrophage-to-myofibroblast transition in chronic liver injury and liver fibrosis. Eur J Med Res. 2023; 28: 502.

35. Kawashima R, Mochida S, Matsui A, YouLuTuZ Y, Ishikawa K, Toshima K. Expression of osteopontin in Kupffer cells and hepatic macrophages and Stellate cells in rat liver after carbon tetrachloride intoxication: a possible factor for macrophage migration into hepatic necrotic areas. Biochem Biophys Res Commun. 1999; 256: 527-31.

36. Wang J, Yuan Z, Zhang H, Wu Q, Miao Y, Xu Y. Obeticholic acid aggravates liver injury by up-regulating the liver expression of osteopontin in obstructive cholestasis. Life Sci. 2022; 307: 120882.

37. Lee TY, Leu YL, Wen CK. Modulation of HIF-1α and STAT3 signaling contributes to anti-angiogenic effect of YC-1 in mice with liver fibrosis. Oncotarget. 2017; 8(: 86206-86216.

38. Calmus Y, Poupon R. Shaping macrophages function and innate immunity by bile acids: mechanisms and implication in cholestatic liver diseases. Clin Res Hepatol Gastroenterol. 2014; 38: 550-6.

39. Gong Z, Zhou J, Zhao S, Tian C, Wang P, Xu C. Chenodeoxycholic acid activates NLRP3 inflammasome and contributes to cholestatic liver fibrosis. Oncotarget. 2016; 7: 83951-83963.

40. Chen G, Zhang H, Ye J. Determination of baicalein, baicalin and quercetin in Scutellariae Radix and its preparations by capillary electrophoresis with electrochemical detection. Talanta. 2000; 53: 471-9.

41. Kong W, Li Z, Xiao X, Zhao Y. Quality control for Coptidis rhizoma through the determination of five alkaloids by HPLC-ELSD coupled with chemometrics. Nat Prod Res. 2010; 24: 1616-29.

42. Lin Z, Qiu S, Wufuer A, Shum L. Simultaneous determination of glycyrrhizin, a marker component in radix Glycyrrhizae, and its major metabolite glycyrrhetic acid in human plasma by LC-MS/MS. J Chromatogr B Analyt Technol Biomed Life Sci. 2005; 814: 201-7.

43. Guo Z, Jin Q, Fan G, Duan Y, Qin C, Wen M. Microwave-assisted extraction of effective constituents from a Chinese herbal medicine Radix puerariae. Analytica chimica acta. 2001; 436: 41-47.

44. Noh JW Kwon OJ Lee B. The Immunomodulating Effect of Baicalin on Inflammation and Insulin Resistance in High-Fat-Diet-Induced Obese Mice. Evid Based Complement Alternat Med. 2021; 2021: 5531367.

45. Noh J, Yang H, Jun M, Lee B. Puerarin Attenuates Obesity-Induced Inflammation and Dyslipidemia by Regulating Macrophages and TNF-Alpha in Obese Mice. Biomedicines. 2022; 10: 175.

46. Wang Y, Zhou X, Zhao D, Wang X, Gurley EC, Liu R. Berberine inhibits free fatty acid and LPS-induced inflammation via modulating ER stress response in macrophages and hepatocytes. PLoS One. 2020; 15: e0232630.